Early View publication on
www.wileyonlinelibrary.com
(issue and page numbers not yet assigned;
citable using Digital Object Identifier – **DOI**)

J. Biophotonics 1–9 (2012) / **DOI** 10.1002/jbio.201200049

Journal of
BIOPHOTONICS

FULL ARTICLE

Tailoring the spectral response of liquid waveguide diagnostic platforms

Yue Zhao[1], *Brian Phillips*[1], *Damla Ozcelik*[2], *Joshua Parks*[2], *Philip Measor*[2], *David Gulbransen*[1], *Holger Schmidt*[2], *and Aaron R. Hawkins*[*,1]

[1] ECE Department, Brigham Young University, 459 Clyde Building, Provo, UT 84602, USA
[2] School of Engineering, University of California Santa Cruz, 1156 High Street, Santa Cruz, CA 95064, USA

Received 19 March 2012, revised 14 April 2012, accepted 17 April 2012
Published online 18 May 2012

Key words: integrated optics, optofluidics, hollow waveguides, filter, signal-to-noise ratio

Liquid filled waveguides that form the basis for on-chip biophotonics diagnostic platforms have primarily found application in fluorescence and Raman spectroscopy experiments that require sensitive discrimination between weak analyte signals and a variety of background signals. Primary sources of background signal can include light from excitation sources (strong, narrow frequency band) and photoluminescence generated in waveguide cladding layers (weak, wide frequency band). Here we review both solid and liquid core filtering structures which are based on anti-resonant reflection that can be integrated with waveguides for attenuating undesirable optical bands. Important criteria to consider for an optimized biosensor include cladding layer materials that minimize broad-spectrum photoluminescence and optimize layer thicknesses for creating a desired spectral response in both solid and liquid guiding layers, and a microfabrication process capable of producing regions with variable spectral response. New results describing how spurious fluorescence can be minimized by optimized thermal growth conditions and how liquid-core filter discrimination can be tuned with liquid core waveguide length are presented.

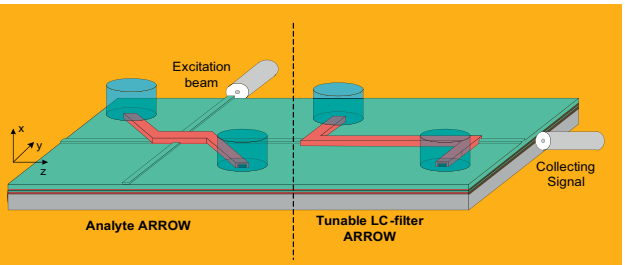

Z-mask ARROW device.

1. Introduction

The chip-based diagnostic platforms discussed here belong to a field of research known as optofluidics. Optofluidic devices combine integrated optics and microfluidics. They can be both optically and fluidically configured, making them advantageous for manipulating and interrogating biological samples in aqueous solutions. Recent applications include biochemical sensing, chemical synthesis and analytical chemistry [1, 2].

Liquid-core waveguides, which allow optical mode guiding along a liquid-filled channel, are key optofluidic elements. A sensing platform based on both liquid-core and solid-core antiresonant reflecting optical waveguides (ARROWs) was proposed by Schmidt et al. in 2005 [3]. The cladding layers of ARROW waveguides are designed to confine light

* Corresponding author: e-mail: hawkins@ee.byu.edu, Phone: +1 801 422 8693, Fax: +1 801 422 0201

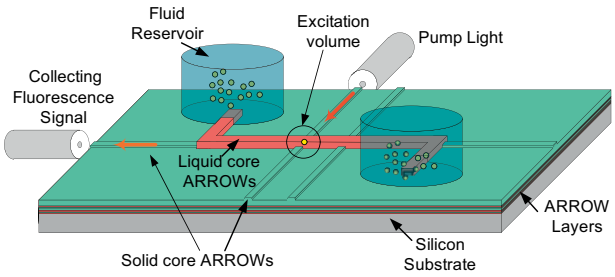

Figure 1 (online color at: www.biophotonics-journal.org) Diagram of ARROW sensing platform.

within a low-index liquid-filled core with a leaky mode. As shown in Figure 1, solid-core waveguides are employed to propagate optical signals on and off the chip and into and out of the liquid waveguides. The ARROW sensing platform has been demonstrated for both fluorescence [4] and surface-enhance Raman scattering (SERS) [5] detection.

In previous work, hollow core ARROWs have been used to analyze viruses, liposomes, ribosomes, and DNA oligonucleotides. When used as a fluorescence sensor, fluorophores are excited when they pass through the perpendicular intersection of solid and liquid cores. Fluorescence signals can be passed along the length of the liquid core and collected by an off-chip detector. Sensitive discrimination between weak analyte signals and a variety of background signals is required, especially for high-sensitivity single molecule detection.

Two sources contribute to the background noise. One of them is the photoluminescence (PL) (weak, wide band) generated from the cladding materials. The other comes from the excitation sources (strong, narrow band). This paper reviews techniques to minimize both detrimental effects by reducing the PL from the cladding layers and incorporating on-chip filtering to remove scattered excitation light from the fluorescence signal. In addition, we introduce on-chip spectral filtering in a dedicated liquid-core filter waveguide.

2. Cladding layers photoluminescence

2.1 Photoluminescence of SiO_2, Si_3N_4, and Ta_2O_5

Photoluminescence is produced in ARROW waveguides when cladding materials absorb photons from an excitation beam and then re-radiate red-shifted photons. Quantum mechanically, this can be described as an excitation to a higher energy state, nonradiative relaxation to a metastable, intermediate level, and then a return to a lower energy state accompanied by the emission of a photon. For the ARROW platform, the PL can be produced in the same wavelength range as analyte fluorescence and thus cannot be filtered without losing fluorescence signal, subsequently limiting the signal-to-noise ratio (SNR). For example, when exciting at 633 nm, the relevant photoluminescence range for cladding materials of ARROW waveguides covers a range of 30–70 nm red-shifted relative to the excitation wavelength, determined by standard fluorophores and matching fluorescence bandpass filters. For an excitation at 633 nm (HeNe laser), this corresponds to a range of interest from 660 to 700 nm.

SiN, SiO_2 and Ta_2O_5 are optically transparent in the visible range and have refractive indices compatible with ARROW claddings. However, as Figure 2 shows, the PL for SiN is higher than that of SiO_2 and Ta_2O_5 in most of the important wavelength span from 660 to 700 nm.

The PL of the amorphous SiN film is dominated by confined excitations within Si quantum dots and defects [6]. Since high index nitride films have more silicon than low index films [7], it is likely that the concentration of PL centers in the film increases due to a greater relative numbers of silicon atoms. Different from SiN films, the PL for Ta_2O_5 films in this range originates from the oxygen-defect level of the TaO_x components [8]. Frequently, as-deposited films consist of fully oxidized Ta_2O_5 and TaO_x ($x < 2.5$) suboxides. The existence of TaO_x leads to oxygen deficiency [9, 10] in the films. The dangling bonds of Ta^+ offered by oxygen deficiencies can potentially trap electrons during conduction band to valence band transitions and emit PL [11]. The metastable trap levels correspond to ionization energies of the oxygen deficiencies.

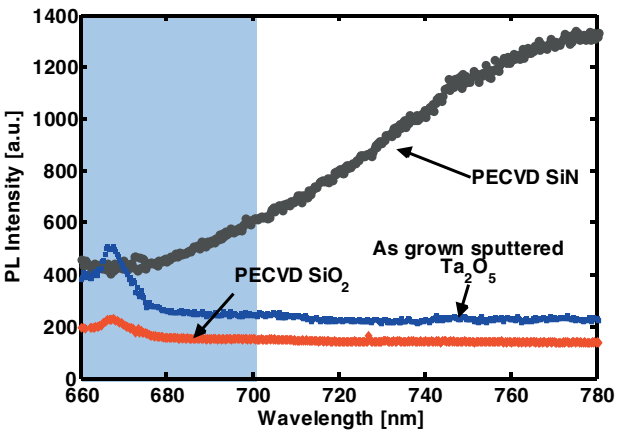

Figure 2 (online color at: www.biophotonics-journal.org) Photoluminescence of PECVD (plasma enhanced chemical vapor deposition) SiN and SiO_2 films ($T = 250\,^{\circ}C$) and sputtered Ta_2O_5 ($T = 250\,^{\circ}C$), shadow region (660–700 nm). PL was measured from 150 nm films deposited on Si wafers.

Over the past two decades, a large number of deposition methods for Ta_2O_5 thin films have been proposed and applied, including anodic or thermal oxidation of tantalum layers [12], sputtering [13], vacuum evaporation [14], atomic layer deposition [15], and CVD [16]. CVD actually is most widely for Ta_2O_5 deposition, however, the typical precursors, such as Ta $(OC_2H_5)_5$), Ta $(OCH_3)_5$, $TaCL_5$, etc., likely cause high levels of hydrocarbon contaminants [17] (H_2O, CO_2, CO, C_2H_4, CH_4, C_2H_5OH, etc.) which result in high photoluminescence intensitys from films. As a result, RF sputtering with a pure Ta_2O_5 target is preferred for making Ta_2O_5 films with the lowest PL in our range of interest.

2.2 *SiN/SiO$_2$ ARROWs Vs Ta$_2$O$_5$/SiO$_2$ ARROWs*

The construction of ARROW waveguides requires alternating layers of low refractive index and high refractive index dielectric films [3, 18]. Given its low PL, PECVD SiO_2 is an obvious choice for the low index film ($n = 1.45$). SiN and Ta_2O_5 both have high refractive indices ($n = 2.0$ and 2.3 respectively) which make them suitable for ARROW designs, but we would expect Ta_2O_5 based ARROWs to exhibit lower background noise signals. As a comparison, ARROW waveguides were made with both PECVD grown SiN and sputtered Ta_2O_5 films (PECVD SiO_2 was used for the low index dielectric in both cases).

A previously described detection setup was employed [4] to compare the detection sensitivity between the fabricated chips (the total optical throughput from chip edge to edge was approximately 10% for both types). As Figure 3(a) shows, the background noise baseline above the detector dark counts of liquid core ARROWs is reduced by 10× by replacing SiN with Ta_2O_5 films [19]. The concomitant increase in sensing SNR was characterized by introducing fluorescent nanoparticles (100 nm diameter, Tetraspeck, Invitrogen, 1.8×10^{10} particles/mL) into the chip via the reservoir (Figure 1, 10 μL). The particles traveled down the channel using pressure driven flow and were optically excited at the orthogonal hollow core/solid core interface. The particle fluorescence was then collected by a single-photon-counting avalanche photodiode. The detected signals for SiN/SiO_2 and Ta_2O_5/SiO_2 devices are shown on Figure 3(b) and 3(c) (over a 5 second span) respectively, where each spike corresponded to a detected nanoparticle. Over a 40 second timeframe, the number of detected particles for the Ta_2O_5/SiO_2 sample was 948 (spikes were counted as particles only if the SNR was greater than 5), with an average SNR of 126.7. The number of detected particles for the SiN/SiO_2 ARROW sample was 53 (again, spikes were counted as particles only if the

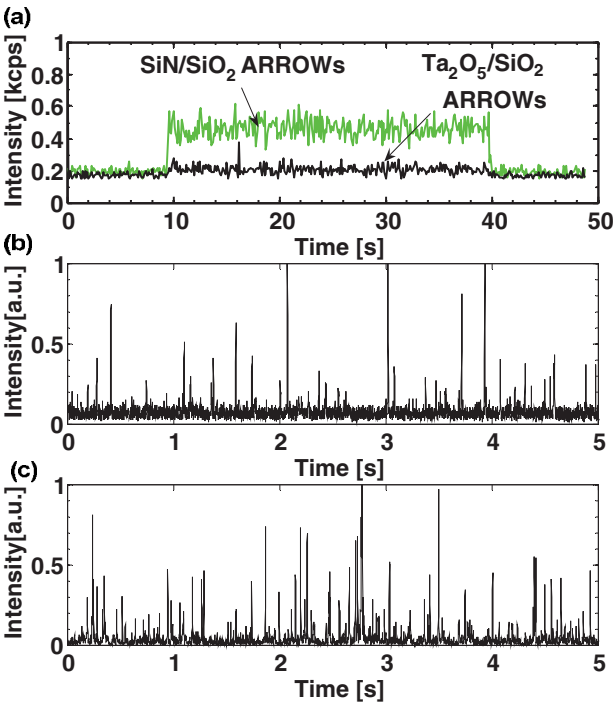

Figure 3 (online color at: www.biophotonics-journal.org) (**a**) Comparison of fluorescence background signals between SiN/SiO_2 samples and Ta_2O_5/SiO_2 samples. In both cases, an excitation laser was turned on at 20 s then off at 40 s. (**b**) Fluorescence signals from excited Tetraspeck nanoparticles in the excitation volume on SiN/SiO_2 ARROWs. (**c**) Fluorescence signals from excited Tetraspeck nanoparcles in the excitation volume on Ta_2O_5/SiO_2 ARROWs. (Reprinted from [19] with permission from the American Physical Society.)

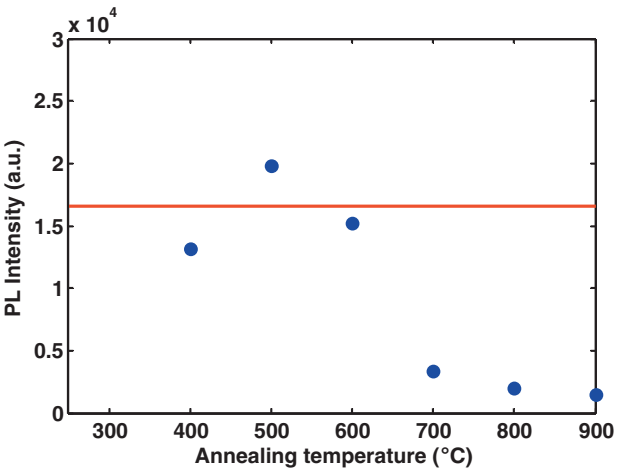

Figure 4 (online color at: www.biophotonics-journal.org) Photoluminescence of Ta_2O_5 films: including as-deposited (grey horizontal line) and post-annealed samples at different temperatures in a N_2 furnace (blue circle dots).

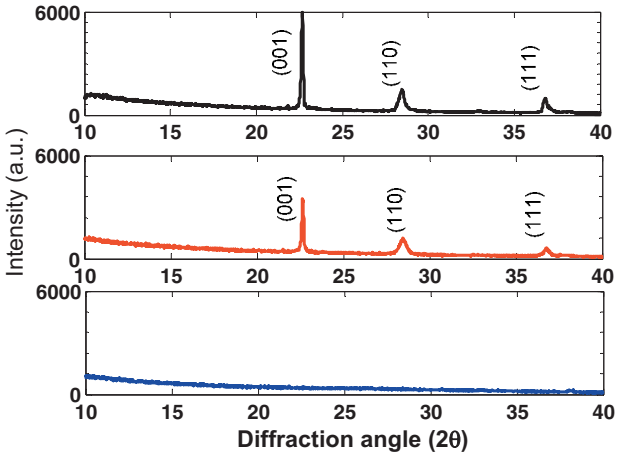

Figure 5 (online color at: www.biophotonics-journal.org) X-ray diffraction pattern of sputtered Ta_2O_5: as grown film (bottom), 700 °C annealed (middle) and 900 °C annealed (top).

SNR was greater than 5), with an average SNR of 10.3.

As stated earlier, the light emission of TaO films in the red light wavelength regime mainly arises from the phase transition from TaO_x to Ta_2O_5. This actually provides a potential way to decrease the PL intensity of TaO films and further improve the SNR of sensing platforms. In the past, research has been done to reduce the PL intensity by thermal [8] or plasma annealing [20]. The thermal annealing method is studied here for as-sputtered films due to the ready availability of a thermal annealing furnace. Seven films (sputtered Ta_2O_5 film of 150 nm thickness) were thermal annealed in a N_2 environment at various temperatures for 30 minutes. Figure 4 shows the integral of the PL intensity in the range of 660–700 nm for all the samples. The PL level of the non-annealed (as-grown) reference sample is represented by the horizontal line. The graph reveals that the PL intensity remains essentially unaffected by the annealing process, but then drops dramatically when the samples were annealed above 700 °C. At the annealing temperature of 900 °C, the PL for a Ta_2O_5 film decreased by 11.2 fold compared to an as-grown film. According to previously reported results, the sputtered Ta_2O_5 film remains amphorous until it is annealed at temperatures above 700 °C [21]. This matches the X-ray diffraction results shown in Figure 5. The peaks in the curves (top and bottom) indicate that the amorphous structure was crystallized into the β-Ta_2O_5 phase when the temperature reaches 700 °C. For crystalline tantalum oxide films, the stoichiometry is improved and the contributions of tantalum suboxides are largely reduced. The PL intensity is therefore minimized since the dangling bonds provided by oxygen deficiencies decrease dramatically. Future, ultra-low background noise ARROWs will take advantage of this annealing effect in the Ta_2O_5 cladding layers.

3. Integrated optical filters

From the discussion above, the ARROW platform has demonstrated high sensitivity single-particle detection capabilities by lowering weak wideband PL noise from the cladding materials. At the same time, optical filters are required to reject scattered high-intensity and narrow-band excitation light and pass the low-intensity signals of interest. The intrinsic wavelength dependence of the underlying interference-based guiding provides a straightforward method for integrating spectral filters on the optofluidic chips. ARROW waveguides confine light with low loss propagation by using antiresonant layers as cladding materials. However, one of the cladding layers can be designed to be resonant to a specific wavelength, leading to its rejection in the waveguide. In this section, we review previous approaches to creating a wideband spectral response using integrated solid-core (SC) and liquid-core (LC) ARROW filter devices.

3.1 Solid-core notch filters

SC notch filters have been integrated on ARROW-based optofluidic chips to specifically reject pump light (HeNe excitation 632.8 nm) while maintaining low loss propagation for longer wavelength fluorescence signals [22]. As Figure 6 shows, broadband antiresonant layers and filter layers were selectively deposited at different regions of an ARROW chip.

Creation of selectively defined regions was accomplished by a lift-off method using a combination of SU-8 and PMGI (LOR 30A/polymethylglutarimide, Microchem) photoresist (Figure 7). During the

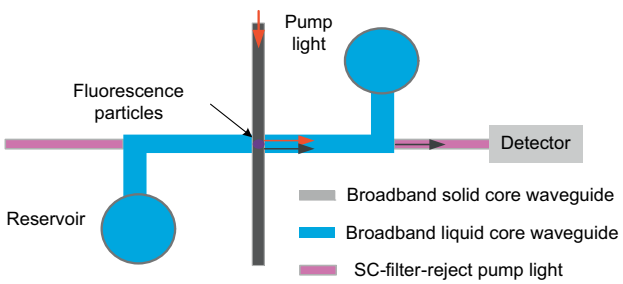

Figure 6 (online color at: www.biophotonics-journal.org) Illustration of an ARROW sensing chip with solid core notch filters.

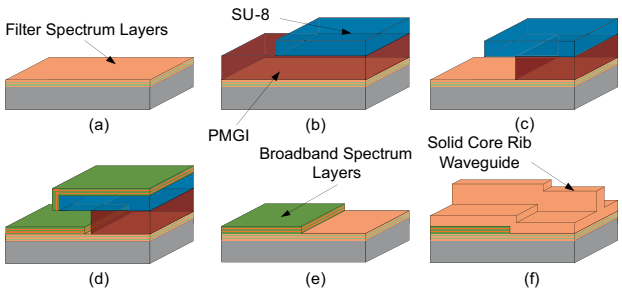

Figure 7 (online color at: www.biophotonics-journal.org) Fabrication process of lift-off SC notch filter (Reprinted from [22] with permission from the Optical Society of America.)

notch filter integration process, dielectric layers that serve as filters are first deposited on a silicon substrate. A layer of PMGI (deep UV-photo-definable) is then deposited, followed by a SU-8 cap-on mask finished by photolithography. Then PMGI is exposed by deep UV with the cap-on SU-8 mask and developed in AZ300 MIF developer. Dielectric films designed for guiding light in a broadband spectrum are then deposited on the whole substrate. Since the lift-off polymer creates a reproducible undercut profile, a natural break occurs at the boundaries which helps to lift off the films cleanly in the resist stripper (1165, Shipley). A thick top layer of SiO_2 is then deposited over the structure and a solid-core rib waveguide is defined using an ICP RIE process.

To characterize the spectral response of an ARROW chip with these SC filters, a white-light source (475 to 950 nm) and detection setup was used and Alexa 647 fluorophores were introduced into the chip

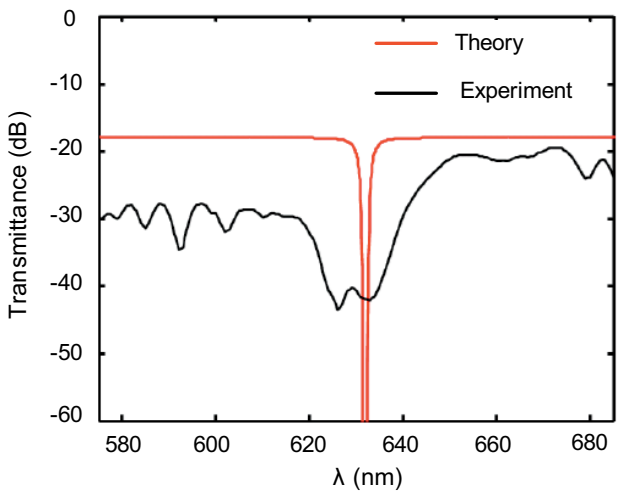

Figure 8 (online color at: www.biophotonics-journal.org) Simulated (red) and resulting (black) spectrum transmission across entire chip with integrated SC filters. (Reprinted from [22] with permission from the Optical Society of America.)

to produce fluorescence signals [22]. As shown in the measured transmission spectrum (Figure 8), the SC filter produces a rejection of ~2 dB/mm with a linewidth as low as 20 nm at 632.8 nm for an integrated ARROW platform. This is comparable to recent inexpensive integrated filters obtaining ~1 dB/mm rejection using long period grating technologies [23], but the length of filtering waveguides is an important consideration in platform implementation and higher rejection values are desirable to minimize chip dimensions.

3.2 *Liquid-core filters*

An alternative approach is to build a desired spectral response into the liquid-core waveguide by careful design of the cladding layer thicknesses using the same mechanism as the solid-core ARROWs. Since the filtering will only happen in the liquid-core waveguide, the solid-core design does not need to change and can be independently tuned. There is no need to selectively apply broadband and filter layers at LC and SC sections, the fabrication process is therefore simplified.

Realization of a liquid-core ARROW filter involved a standard sacrificial core procedure clad with alternating thin film dielectric layers of SiO_2 and Ta_2O_5 [24]. LC ARROW filters were first designed and fabricated on integrated ARROW platforms for FRET (Förster resonance energy transfer) applications [24]. FRET is used to measure small distance change between FRET pairs (donors and acceptors) attached with two different fluorescence dyes. A FRET filter has to be designed to reject the excitation wavelength λ_{ex} and pass both donor wavelength λ_d and acceptor wavelength λ_a. The requirement for multiple wavelengths can be achieved by using three strict tolerance resonant layers.

For a specific application using the common Cy3 and Cy5 FRET pair, λ_{ex}, λ_d and λ_a are 532, 570 and 690 nm respectively. With a water core ($n = 1.33$), the layers from the silicon substrate are designed with a sequence of SiO/SiN/SiO/SiN/SiO/SiN/core/SiN/SiO/SiN/SiO/SiN/SiO: 213/768/213/768/213/768/4000/121/369/121/369/121/179 (units in nm). Spectral characterization was done using a previously described setup [24]. As shown in Figure 9, the calculated transmission spectrum shows excellent agreement with the experimental background normalized transmittance for a 4 mm-long water-filled waveguide. The integrated LC filter shows a donor channel (channel D) extinction of 36 dB and an acceptor channel (channel A) extinction of 37 dB for the 4 mm long samples (9.25 dB/mm). The FSR (free spectral range) of 76 nm is very close to the expected 73 nm and allows for more collected light

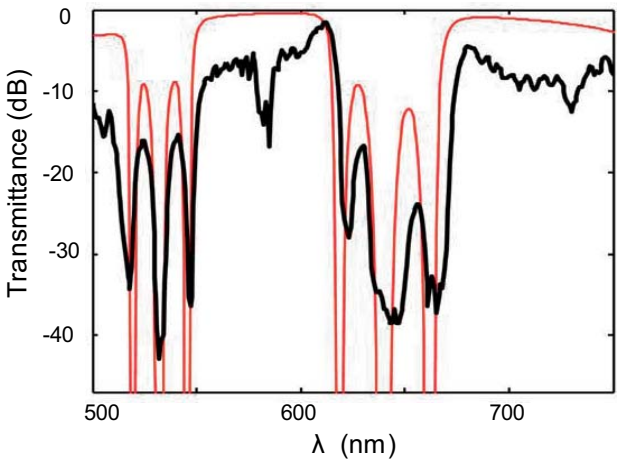

Figure 9 (online color at: www.biophotonics-journal.org) Optofluidic filter experimental (thick line) and calculated design (thin line) spectral response for a 4 mm long liquid-core ARROW waveguide. (Reprinted from [24] with permission from the Royal Society of Chemistry.)

than a discrete passband filter. In order to determine the SNR improvement using the LC filters, fluorescent nanoparticles (100 nm diameters, Tetraspeck, Invitrogen) were introduced into the liquid-core via the reservoir. The average SNR increased from 15 to 70 with an integrated LC filter (4.7 × improvement).

While this previous work has shown that liquid-core filter sections deliver excellent performance without increasing fabrication complexity, it is generally desirable to separate detection and signal processing (filtering) zones on a chip. To this end, we have implemented LC filters in a novel configuration. Figure 10 illustrates that the overall device consists of two separate liquid-core portions. The first, labeled Analyte ARROW on the left side is used to flow specific analytes into the sensing region. This sensing region consists of a short section of liquid-core waveguide oriented in the z direction, as well as a perpendicular solid-core waveguide for delivery of pump light from an off-chip laser source. The fluorescence or Raman signal to be detected is coupled into the liquid-core waveguide mode, and propagates

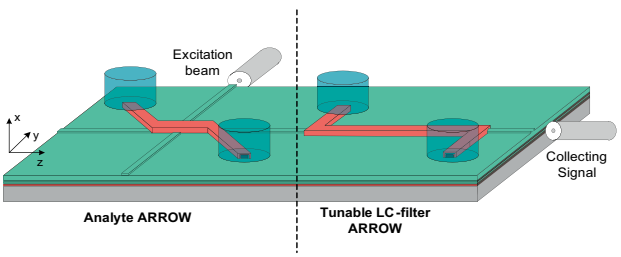

Figure 10 (online color at: www.biophotonics-journal.org) Z-mask ARROW device: left, analyte ARROW waveguide; right, Tunable liquid-core filter ARROW.

laterally through a solid-core waveguide. Comparing with previous devices with longer LC waveguides (4 mm), the short length (300 μm) reduces the propagation loss and therefore can transmit more fluorescence signals for sensing. The analyte liquid can now be chosen without affecting the spectral filtering performance. The solid-core waveguide carries the signal as well as scattered excitation signal to the liquid-core filter ARROW on the right side of Figure 10. This independent liquid-core section can be much longer to maximize rejection of the scattered excitation light, while passing the fluorescent or Raman signal for off-chip detection. Although this type of sensing platform has different configurations, it does not cause more complex fabrication steps, instead, it can be fabricated using the same method previous described.

During fabrication of these devices, it was found that the piranha solution (H_2SO_4:H_2O_2) used to remove the sacrificial core had an etching effect on the low-density PECVD SiN cladding layers immediately surrounding the waveguide core. To characterize this etching process, single films of PECVD SiN were placed into piranha etchant at 130 °C for a total duration of 2 weeks. Sample roughness and thickness was measured using atomic force microscopy (AFM) and ellipsometry, respectively. The results of these measurements are shown in Table 1.

From the recorded data, the piranha etchant appears to slowly react with the films over a period of 5 days, before it begins to remove and roughen the SiN cladding layer. This roughness increases the loss of the liquid-core waveguides, drastically affecting the analyte waveguide of the ARROW, due to the sacrificial core being removed much sooner than the filter waveguide of the ARROW. This etching process was mitigated by depositing a thin SiO_2 cladding layer immediately surrounding the sacrificial core. Provided the SiO_2 layer is less than ∼50 nm in thickness, it will have negligible effect on the waveguiding properties of the liquid-core ARROW as shown in Figure 11. The optimized piranha etchant shows no measureable etching of the PECVD SiO_2 films over a similar 2 week experiment.

For characterization of the filter mechanism, various devices consisting of different liquid-core filtering lengths were constructed ($L = 4,\ 5,\ 6,\ 7$ mm) with a layer sequence of SiO/SiN/SiO/SiN/SiO/SiN/

Table 1 SiN/Piranha reactivity.

Day	Etched Thickness	Roughness [nm rms]
0	0 nm	0.25
3	0 nm	0.33
5	0 nm	0.33
10	20 nm	2.25
14	45 nm	4.00

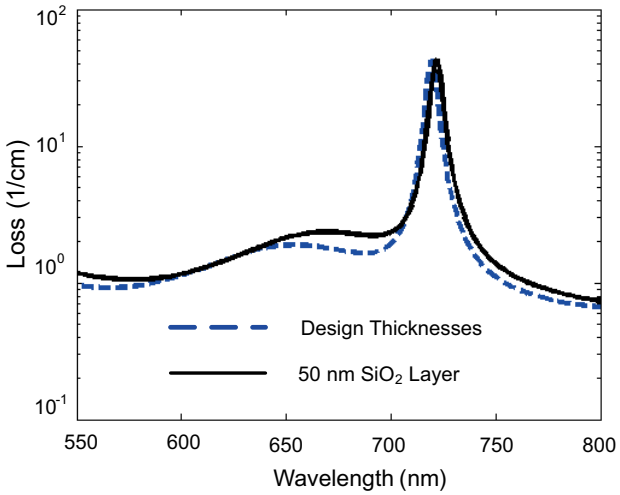

Figure 11 (online color at: www.biophotonics-journal.org) Calculated liquid-core loss coefficient for the design layer thickness (dashed) and with a 50 nm SiO_2 cladding layer immediately surrounding all four sides (solid).

core/SiN/SiO/SiN/SiO/SiN/SiO: 296/115/230/296/115/4000/128/368/128/386/128/1688 (units in nm). The spectral response of the LC tunable filters was measured using the same white-light setup previously used for SC notch filters. Simulated and measured results of a z-mask device with a 4mm-long LC-filter ARROW filled with 70% EG (ethylene glycol)-water solution ($n = 1.4$) are shown in Figure 12. From the measured curve, it can be seen that a 4 mm-long LC-filter ARROW produced a peak rejection of 18.9 dB with a linewidth of 12 at 646 nm compared to a passband of 600 ∼ 640 nm. The linewidth broadening results from a filter thickness deviation during the fabrication process. In addition, the peak rejection of all devices versus filter length is shown in Figure 13. The observed linear increase in total rejection with the length of the filter section suggests that the device quality did not degrade due to the longer etching times for the longer filter sections. At ∼4.7 dB/mm, these longer LC filters show a 2.3× improvement in rejection and a 1.7× reduction in linewidth over SC ARROW filters. If the LC notch filters are made with longer length and the same material system, they can provide a greater rejection than previous described LC FRET filters while collecting more fluorescence signals. Table 2 summarizes the performance of the various filter types.

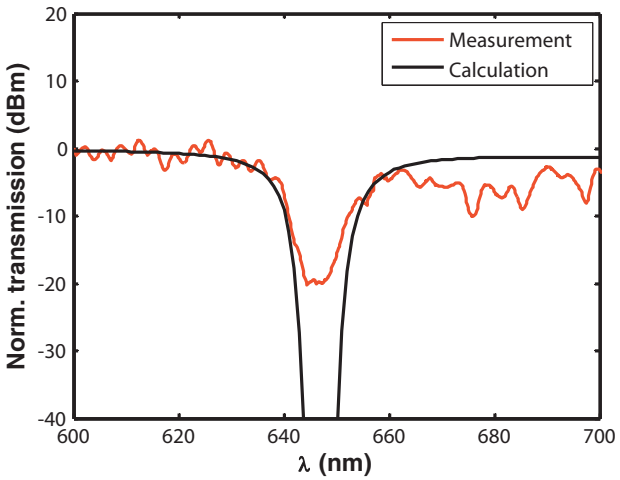

Figure 12 (online color at: www.biophotonics-journal.org) Spectral response of 4 mm-long LC ARROW filter: calculated (black) and measured curve (red) filled with 70% EG-water solution.

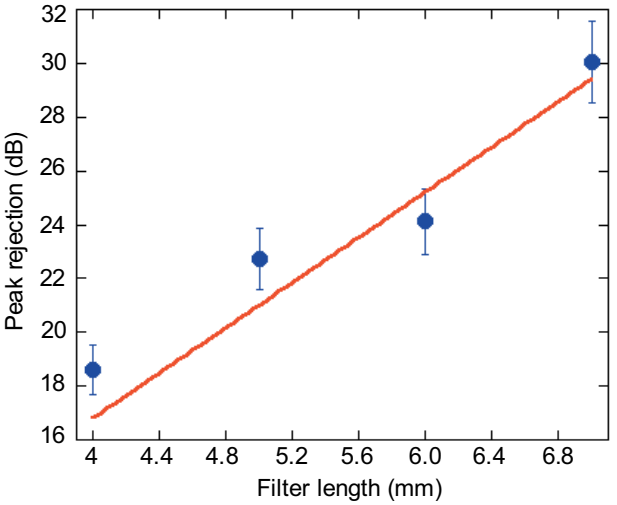

Figure 13 (online color at: www.biophotonics-journal.org) Optical rejection versus filter length for LC ARROW filters filled with 70% EG-water solution.

Table 2 Comparison between different on-chip filter types.

Filter type	norm. rejection (dB/mm)	peak rejection (dB)
SC notch	2	8
LC notch (SiN)	4.7	30
LC FRET (Ta_2O_5)	9.25	37

4. Conclusions

In conclusion, the sensitivity of ARROW sensing platforms can be improved substantially by minimizing unwanted background signals.

Photoluminescence caused by the optofluidic chip materials was reduced by replacing SiN films with Ta_2O_5 films serving as cladding materials. Since

Ta_2O_5 films shows lower PL background noise than SiN films in a relevant wavelength range, ARROW chips with the material system of Ta_2O_5/SiO_2 demonstrate an enhanced signal-to-noise ratio for fluorescent particle detection. Moreover, high-temperature annealing methods of TaO films resulted in a phase transition to a crystalline state, accompanied by a drastic suppression of the photoluminescence.

SC and LC notch filters were investigated to reduce the noise coming from the scattering of a high intensity fluorescence excitation beam. On-chip spectral filtering can be achieved by selective layer design in the solid-core waveguides or by careful design of the liquid-core cladding layer thicknesses. Both lead to functional filters and improved SNR for fluorescent particle detection. In comparison, a new configuration with separate analyte section and LC filter section exibits increased rejection, smaller linewidths, and larger free spectral range than found in previous SC filters.

So far, the two-section LC filter ARROW has only been fabricated with the SiO_2/SiN material system. In the future, the SNR of the ARROW sensing platform can be maximized by combining high-temperature Ta_2O_5/SiO_2 waveguide layers with dedicated LC filter sections.

Acknowledgements This work was supported by the NIH/NIBIB, NSF, and the W. M. Keck Center for Nanoscale Optofluidics at the University of California at Santa Cruz. B. S. P. acknowledges support from the SMART Scholarship for Service Program. We would also like to thank Stacey Smith for assistance with X-ray diffraction measurements.

Yue Zhao got her B.S. and M.S. degrees in Huazhong University of Science and Technology, China. She started working in ARROW project since 2006 and received PhD degree in April, 2012. Yue Zhao is currently working as a R&D Process Development Engineer at Micron Technology.

Brian S. Phillips received the B.S. ('07) and Ph.D. ('11) degrees in Electrical and Computer Engineering from Brigham Young University. While a graduate student, he interned with the United States Army at Dugway Proving Grounds developing standoff and point detection systems of simulant chemical and biological aerosols. Dr. Phillips is currently a Senior Member of Technical Staff working in Cybersecurity Research & Development at Sandia National Laboratories.

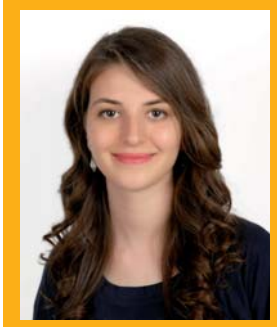

Damla Ozcelik joined the Applied Optics group at University of California, Santa Cruz in 2010. Her research interest includes single bio-particle analysis in optofluidic devices, optical manipulation, and biophotonics.

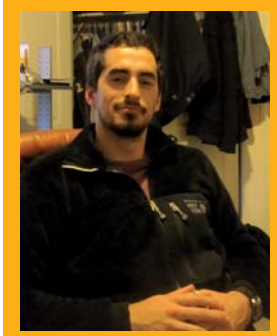

Joshua Parks is a biochemistry Ph.D. student and joined the Applied Optics group in 2010. He obtained a B.S. in Biochemistry from the University of Portland in 2010. His research interests include optical studies on the nanoscale. He is the recipient of a Cota Robles Graduate Fellowship and Nation Science Foundation Graduate Research Fellowship. Josh's research interests include single biomolecule analysis in optofluidic devices and biophotonics.

Philip Measor is a researcher and developer of novel integrated optofluidic devices. He has 33 publications in the field of Optofluidics. He received his B.S. and Ph.D. in Electrical Engineering from UC Santa Cruz in 2004 and 2010, respectively. He also served a postdoctoral role until late 2011. Dr. Measor is now the CEO of LiquiLume Diagnostics where he is leading the efforts to commercialize novel optofluidic technology.

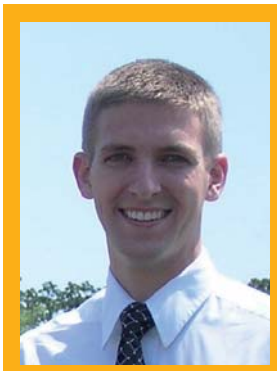

David Gulbransen is an undergraduate student studying in Electrical Engineering at BYU. He joined the Dr. Hawkins's group in 2011, conducting research in BYU's IML for ARROW project.

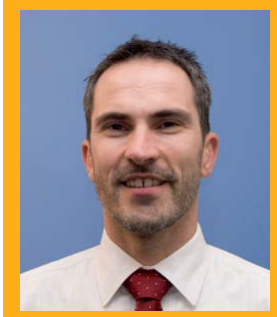

Holger Schmidt received his Ph.D. degree in electrical and computer engineering from the University of California, Santa Barbara, in 1999. After serving as a Postdoctoral Fellow at M.I.T., he joined the University of California, Santa Cruz, in 2001, where he is professor of electrical engineering and Director of the W.M. Keck Center for Nanoscale Optofluidics. His research interests include optofluidic devices, single-photon nonlinearities, and nano-magneto-optics. He received a National Science Foundation CAREER Award in 2002 and a Keck Futures Nanotechnology Award in 2005.

Aaron R. Hawkins received the B.S. degree in applied physics from the California Institute of Technology, Pasadena, in 1994 and the M.S. and Ph.D. degrees in electrical and computer engineering from the University of California, Santa Barbara, in 1996 and 1998, respectively. He was a co-founder of Terabit Technology and later worked at CIENA and Intel. He is currently a Professor with the Electrical and Computer Engineering Department, Brigham Young University, Provo, UT. He has authored or coauthored over 250 technical publications.

References

[1] X. Fan and I. M. White, Nat. Photonics **5**(10), 591–597 (2011).
[2] H. Schmidt and A. R. Hawkins, Nat. Photonics **5**, 598–604 (2011).
[3] H. Schmidt, D. L. Yin, J. P. Barber, and A. R. Hawkins, Ieee J. Sel. Top. Quant. **11**(2), 519–527 (2005).
[4] D. Yin, E. J. Lunt, M. I. Rudenko, D. W. Deamer, A. R. Hawkins, and H. Schmidt, Lab Chip **7**(9), 1171–1175 (2007).
[5] P. Measor, L. Seballos, D. Yin, J. Z. Zhang, E. J. Lunt, A. R. Hawkins, and H. Schmidt, Appl. Phys. Lett. **90**(21), 211107 (2007).
[6] B. Rezgui, A. Sibai, T. Nychyporuk, M. Lemiti, and G. Brémond, J. Lumin. **129**(12), 1744–1746 (2009).
[7] W. A. P. Classen, W. G. J. N. Valkenburg, F. H. P. M. Habraken, and Y. Taminga, J. Electrochem. Soc. **130**(12), 2419–2423 (1983).
[8] M. Zhu, Z. Zhang, and W. Miao, Appl. Phys. Lett. **89**(2), 021915 (2006).
[9] H. Sawada and K. Kawakami, J. Appl. Phys. **86**(2), 956–959 (1999).
[10] R. Ramprasad, J. Appl. Phys. **94**(9), 5609 (2003).
[11] R. S. Devan, W. D. Ho, C. H. Chen, H. W. Shiu, C. H. Ho, C. L. Cheng, S. Y. Wu, Y. Liou, and Y. R. Ma, Nanotechnology **20**(44), 445708 (2009).
[12] C. J. Dell'Oca and L. Young, J. Electrochem. Soc. **117**(2), 1548–1551 (1970).
[13] E. Atanassova, T. Dimitrova, and J. Koprinarova, Vacuum **46**(8–10), 889–891 (1995).
[14] J. Hudner, P. E. Hellberg, D. Kusche, and H. Ohlsen, Thin Solid Films **281–282**, 415–418 (1996).
[15] M. Ylilammi, J. Electrochem. Soc. **142**(7), 2474–2479 (1995).
[16] G. Q. Lo, D. L. Kwong, and S. Lee, Appl. Phys. Lett. **60**(26), 3286–3288 (1992).
[17] S. B. Desu, Mater. Chem. Phys. **31**(4), 341–345 (1992).
[18] R. Bernini, E. D. Nuccio, A. Minardo, L. Zeni, and P. M. Sarro, IEEE J. Sel. Top. Quant. Electron. **13**(2), 194–201 (2007).
[19] Y. Zhao, M. Jenkins, P. Measor, K. Leake, S. Liu, H. Schmidt, and A. R. Hawkins, Appl. Phys. Lett. **98**(9), 91104 (2011).
[20] G. B. Alers, R. M. Fleming, Y. H. Wong, B. Dennis, and A. Pinczuk, Appl. Phys. Lett. **72**(11), 1308–1310 (1998).
[21] G. Sethi, B. Bontempo, E. Furman, M. W. Horn, M. T. Lanagan, S. S. N. Bharadwaja, and J. Li, J. Mater. Res. **26**(6), 745–753 (2011).
[22] B. S. Philips, P. Measor, Y. Zhao, H. Schmidt, and A. R. Hawkins, Opt. Express **18**(5), 4790–4795 (2010).
[23] K. P. Lor, Q. Liu, and K. S. Chiang, IEEE Photonics Technol. Lett. **17**(3), 594–596 (2005).
[24] P. Measor, B. S. Phillips, A. Chen, A. R. Hawkins, and H. Schmidt, Lab Chip **11**(5), 899–904 (2011).